Energy & Environmental Science



PAPER View Article Online



Cite this: DOI: 10.1039/d1ee03251h

Mechanistic insights of cycling stability of ferrocene catholytes in aqueous redox flow batteries*

Jian Luo, 📵 a Maowei Hu, a Wenda Wu, a Bing Yuan 📵 ab and T. Leo Liu 📵 *a

Water soluble ferrocene (Fc) derivatives are promising cathode materials for aqueous organic redox flow batteries (AORFBs) towards scalable energy storage. However, their structure–performance relationship and degradation mechanism in aqueous electrolytes remain unclear. Herein, physicochemical and electrochemical properties, battery performance, and degradation mechanisms of three Fc catholytes, (ferrocenylmethyl)trimethylammonium chloride (C_1 -FcNCl), (2-ferrocenyl-ethyl)trimethylammonium chloride (C_2 -FcNCl), and (3-ferrocenyl-propyl)trimethylammonium chloride (C_3 -FcNCl) in pH neutral aqueous electrolytes were systemically investigated. UV-Vis and gas chromatography (GC) studies confirmed the thermal and photolytic C_x -Cp $^-$ ligand dissociation decomposition pathways of both discharged and charged states of C_1 -FcNCl and C_2 -FcNCl catholytes. In contrast, in the case of the C_3 -FcNCl catholyte, the electron-donating 3-(trimethylammonium)propyl group strengthens the coordination between the C_3 -Cp $^-$ ligand and the Fe 3 + or Fe 2 + center and thus mitigates the ligand-dissociation degradation. Consistently, the Fc electrolytes displayed cycling stability in both half-cell and full-cell flow batteries in the order of C_1 -FcNCl < C_2 -FcNCl < C_3 -FcNCl.

Received 16th October 2021, Accepted 3rd February 2022

DOI: 10.1039/d1ee03251h

rsc.li/ees

Broader context

Redox flow batteries (RFBs) are positioned to integrate renewable energy into existing electricity grids. A new generation of aqueous organic RFBs (AORFBs) using sustainable and tunable redox organic molecules holds excellent promise to penetrate scalable energy storage applications. However, the performance of AORFBs is typically limited by the lack of high-performance cathode electrolytes (called catholytes). Thus, it is highly critical to conduct mechanistic studies of catholyte molecules. In-depth understandings of their degradation pathways are essential to developing more robust, energy dense catholyte molecules, paving the road to resilient energy storage performance. We present a comprehensive mechanistic study of water-soluble ferrocene catholytes. This work discloses their thermal and photolytic degradation pathways and molecular engineering solutions for developing stable coordination complex redox active electrolytes. The presented results elucidate valuable design principles to develop advanced coordination complex redox active electrolytes for scalable, long-duration energy storage.

Introduction

Advanced technologies for grid-scale energy storage are broadly demanded to efficiently utilize intermittently available, fluctuating renewable energies such as solar and wind and ensure stable, secured power supply of the electricity grid.¹ Among various electrochemical energy storage technologies, aqueous

technology for renewable energy integration and electricity grid balancing because of their technologic advantages, including decoupled energy and power, high power and energy performance, excellent modularity and scalability, and environmentally friendly aqueous electrolytes.^{1,2}

redox flow batteries (ARFB) have been recognized as a viable

Sustainable and tunable organic and organometallic redoxactive molecules have become increasingly attractive to serve as charge storage materials in ARFBs. In the past ten years, significant progress has been made in the aqueous organic redox flow battery (AORFB) technology. Water-soluble viologen (anolyte), quinone (anolyte and catholyte), henazine (anolyte), TEMPO (catholyte), and ferrocene (catholyte), compounds were developed for AORFB demonstration. However, the most critical roadblock to further

^a The Department of Chemistry and Biochemistry, Utah State University, Logan, 84318, USA. E-mail: Leo.Liu@usu.edu

b State Key Laboratory Base of Eco-Chemical Engineering, College of Chemistry and Molecular Engineering, Qingdao University of Science and Technology, Qingdao 266042, China

[†] Electronic supplementary information (ESI) available: The ferrocene compounds synthesis and characterization, electrochemical study and battery test details, post-cell analysis. See DOI: 10.1039/d1ee03251h

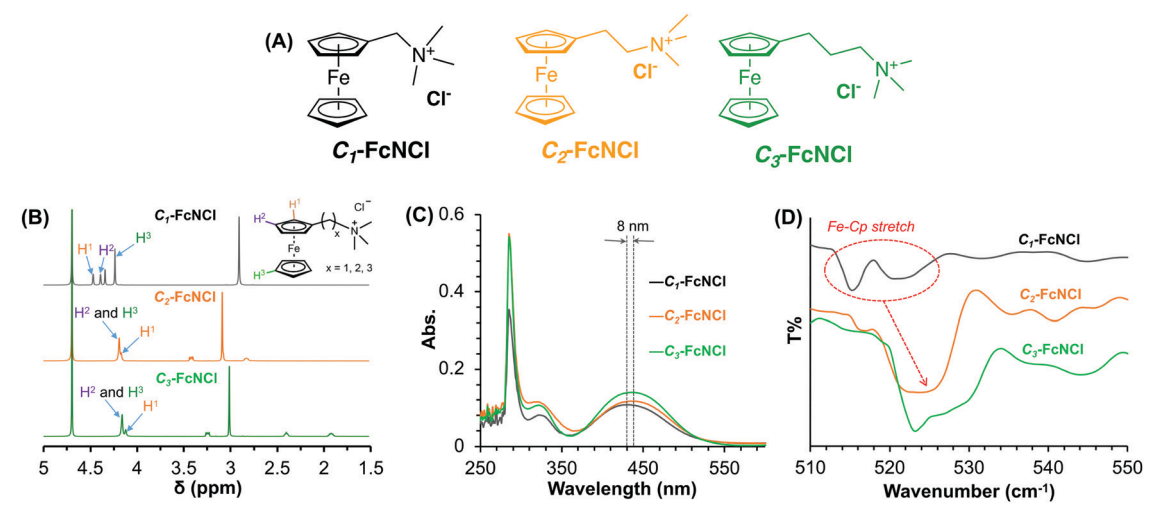


Fig. 1 Spectroscopic studies of the Fc derivatives, C₁-FcNCl (black), C₂-FcNCl (orange), C₃-FcNCl (green). (A) Structures of the Fc derivatives; (B) ¹H-NMR in D₂O; (C) UV-Vis absorption; and (D) ATR-IR spectra.

boost the energy storage performance of AORFBs lies in the lack of stable catholyte materials.²⁸ So far, ferrocene and TEMPO derivatives are common catholyte materials for AORFBs. Despite being extensively used in flow batteries, there are very few mechanistic studies to gain insightful understandings of the chemical stability of catholyte molecules, which is key to developing more advanced catholyte materials.1

In our previous work, we reported a highly water-soluble (ferrocenylmethyl)trimethylammonium chloride (C_1 -FcNCl, Fig. 1A) as a catholyte (4.00 M solubility in water at room temperature) for AORFB applications.7 Paired with methyl viologen (MV) anolyte, the C1-FcNCl/MV AORFB delivered reliable cycling performance and battery efficiency. However, in long-term cycling tests, capacity fading was still observed, specifically, ca. 9.0% capacity decay in 700 charge/discharge cycles at 60 mA cm⁻² current density. Subsequent studies revealed that the derivatives of C1-FcNCl with a longer methylene chain between the Fc and ammonium groups displayed improved cycling performance. 10,27 One argument was that C_1 -FcNCl might undergo a dimerization decomposition mechanism. 10 Instead, Cp ligand exchange with an external ligand such as Cl was proposed as a possible degradation pathway for ferrocenium cation (Fc⁺) in organic solutions in 1972.²⁹ Our recent work also suggested that the ligand dissociation commences the decomposition of ferrocyanide in alkaline solutions.³⁰ Thus, we hypothesize that the Cp ligand dissociation initiates the degradation of ferrocene in organic solutions. We further infer that the charged state, $[C_1$ -FcN $]^{2+}$, of C_1 -FcNCl might follow a similar decomposition mechanism. Furthermore, we envision that ferrocene catholytes can be stabilized by the +I inductive effect of substituted groups of the Cp⁻ ligand. The electron-donating functional groups can increase the binding strength of a Cp⁻ ligand and a Fe³⁺ center and lower the possibility of dissociation of the Cp ligand, thereby suppressing subsequent ligand exchange reactions.

To elucidate the donation effect of the Cp⁻ ligand, we report a systematic study of physiochemical properties, chemical stability, and battery performance of a series of trimethylammonium) alkyl functionalized ferrocene molecules, C_1 -FcNCl, and two derivatives with a purposely designed longer (trimethylammonium)alkyl pendant, (2-ferrocenylethyl)trimethylammonium chloride (C_2 -FcNCl) and (3-ferrocenylpropyl) trimethylammonium chloride (C_3 -FcNCl) (Fig. 1A). Our results revealed that the series displayed increased chemical stability and cycling stability with the increased length of the (trimethylammonium)alkyl pendant and thus the donation strength of the substituted Cp ligand by avoiding the ligand exchange side reaction of the Cp⁻ ligand (Fig. 1). Specifically, a suit of spectroscopic studies elucidated that both thermally and photolytically induced ligand dissociation triggered the chemical decomposition of electron deficient ferrocene electrolytes to iron hydroxide precipitates in the presence of water. The present results highlight the importance of the ligand coordination sphere of the coordination compound based redox active electrolytes regarding their energy storage performance. Paired with a viologen anolyte under pH-neutral conditions, the most stable C_3 -FcNCl catholyte in a 0.50 M AORFB delivered up to an energy efficiency of 91% at 10 mA cm⁻² and capacity retention of 99.998% per cycle or 99.927% per day in 500 cycles.

Results

(trimethylammonium)alkyl group functionalized Fc derivatives (C_x -FcNCl, x = 1, 2, and 3, Fig. 1A), (ferrocenylmethyl)trimethylammonium chloride (C_1 -FcNCl), (2-ferrocenyl-ethyl) trimethylammonium chloride $(C_2$ -FcNCl), and (3-ferrocenyl propyl)trimethylammonium chloride (C_3 -FcNCI) were synthesized (Scheme S1, ESI†) and fully characterized by ¹H-NMR, elemental analysis, UV-Vis, IR, and cyclic voltammetry (CV). Fig. 1B exhibits the ¹H-NMR spectra of the C_x -FcNCl compounds. For C_1 -FcNCl, the proton signals of the (trimethylammonium)methyl group modified Cp ligand possessed much larger chemical shifts than those of the pristine Cp⁻ ligand (δ : H¹-4.47 and H²-4.39 (H²) vs. H³-4.24 in Fig. 1B), which suggests the strong electron-withdrawing effect of the (trimethylammonium)methyl group. In contrast, in C_2 -FcNCl and C_3 -FcNCl compounds, the signal of proton near the

Published on 03 February 2022. Downloaded by Utah State University Eastern Blanding Campus on 2/23/2022 11:58:55 PM.

 C_1 -FcNCl.

higher field than those of the pristine Cp⁻ ligand (H³), indicating 2-(trimethylammonium)ethyl and 3-(trimethylammonium)propyl are electron-donating groups. Smaller chemical shifts of protons on Cp⁻ ligands of C₃-FcNCl (4.14 (H¹) and 4.18 ppm (H² and H³)) than C₂-FcNCl (4.17 (H¹) and 4.20 (H² and H³) indicates the stronger electron-donating capability of 3-(trimethylammonium)propyl group than 2-(trimethylammonium)ethyl group. Fig. 1C shows the UV-Vis absorption of C_x -FcNCl compounds. Three compounds displayed two spin-allowed d-d transitions: 323 and 430 nm for C₁-FcNCl, 321 and 438 nm for C_2 -FcNCl, and 323 and 438 nm for C_3 -FcNCl. The strong absorption around 285 nm is assigned as the overlapped metal-to-ligand charge transfer (MLCT) and ligand-to-metal charge transfer (LMCT). As shown in the IR spectra of C_1 -FcNCl (Fig. 1D, gray curve), two divided Fe^{II}-Cp stretch absorption were observed at 515 cm⁻¹ and 521 cm⁻¹ wavenumbers, corresponding to those two different Cp⁻ ligands.³² However, the same absorption signals were shifted to larger wavenumbers, a broad peak centered on 524 cm⁻¹ for C_2 -FcNCl and 523 cm⁻¹ and 527 cm⁻¹ for C_3 -FcNCl, which indicates the stronger coordination between Fe^{II} center and substituted Cp⁻ ligands in C_2 -FcNCl and C_3 -FcNCl than that of

(trimethylammonium)alkyl functional groups (H1) shifted to a

Physicochemical properties of the C_x -FcNCl compounds regarding flow battery performance were systemically investigated (Table 1). With the extension of the alkyl chain between the Fc redox center and trimethylammonium functional group, water solubility gradually decreased from 4.00 M (i.e., a capacity of 107.2 Ah L^{-1}) of C_1 -FcNCl to 2.60 M (69.7 Ah L^{-1}) of C_2 -FcNCl and 2.30 M (61.6 Ah L⁻¹) of C_3 -FcNCl at room temperature. Ion conductivities of the Fc derivatives in water were measured at a concentration range from 0.01 M to 2.00 M (Fig. S1A, ESI†). Even in the absence of a supporting electrolyte, aqueous solutions of C_x -FcNCl demonstrated high conductivities of up to 50.0 mS cm⁻¹ at room temperature. Liner relationship between conductivity and concentration was observed in the 0.01 M to 0.20 M concentration range. The slope of conductivity versus concentration plot is calculated as molar ion conductivity of the C_x -FcNCl compounds (Fig. S1B, ESI†). These three Fc derivatives displayed comparable molar ion conductivity $(63.0 \text{ S cm}^2 \text{ mol}^{-1} \text{ for } C_1\text{-FcNCl}, 63.7 \text{ S cm}^2 \text{ mol}^{-1} \text{ for }$ C_2 -FcNCl, and 61.4 S cm² mol⁻¹ for C_3 -FcNCl, Table 1). The high ion conductivities of C_r -FcNCl compounds are beneficial for boosting the energy and power performance of related AORFBs.

Electrochemical studies of the Fc derivatives were conducted in a 0.50 M NH₄Cl supporting electrolyte. As shown in Fig. 2A,

three compounds exhibited a reversible Fe3+/2+ redox wave in their cyclic voltammetry, i.e., 0.61 V (vs. NHE) for C_1 -FcNCl, 0.44 V for C_2 -FcNCl, and 0.37 V for C_3 -FcNCl. CV scan rate dependence studies indicate that the reversible Fe^{3+/2+} redox process is a diffusion-controlled process (Fig. S2D, ESI†). The heterogeneous standard electron transfer rate constants k^0 of C_x -FcNCl compounds were determined by Nicholson's method (Fig. S2, ESI†).³³ Fast electron transfer rate constants (k^0) were calculated (0.126 cm s⁻¹ for C_1 -FcNCl, 0.288 cm s⁻¹ for C_2 -**FcNCl**, and 0.193 cm s⁻¹ for C_3 -FcNCl, respectively). Linear sweep voltammetry (LSV) studies using a glassy carbon rotation disc electrode were performed to measure the diffusion coefficients (D) of C_x -FcNCl compounds (Fig. S3, ESI†). The diffusion coefficients (D) were calculated by Levich equation as 6.80 \times $10^{-6} \text{ cm}^2 \text{ s}^{-1} \text{ for } C_1\text{-FcNCl}, 6.10 \times 10^{-6} \text{ cm}^2 \text{ s}^{-1} \text{ for } C_2\text{-FcNCl},$ and 5.78×10^{-6} cm² s⁻¹ for C_3 -FcNCl in 0.50 M NH₄Cl aqueous solution, respectively. The gradual decrease of diffusion coefficients (D) from C_1 -FcNCl to C_2 -FcNCl and C_3 -FcNCl is likely due to the increase of Fc molecular size with the extension of the alkyl chain.

Battery performance of the C_r -FcNCl catholytes in AORFB was evaluated using a half-cell RFB approach (Table 2), which has been confirmed as an efficient method for assessing the performance of a redox active electrolyte. 30 The battery studies were conducted in the dark to avoid the possible negative impacts of light exposure. As shown in Fig. 2B, the half-cell RFBs were tested using 0.50 M discharged state, $[C_x$ -FcN]⁺, and 0.5 M charged state, $[C_x$ -FcN]²⁺, in a 1.0 M NH₄Cl supporting electrolyte as a catholyte and an anolyte, respectively. The RFBs were performed at a current density from 10 mA cm⁻² to 50 mA cm⁻² with ± 0.30 V cutoff voltage. As shown in Fig. 2C, C_1 -FcNCl half-cell RFB showed slight capacity decay over 5 continuous cycles at 10 and 20 mA cm⁻² current densities. However, stable capacity retention was observed in C_2 -FcNCl and C_3 -FcNCl half-cell RFBs at each current density from 10 mA cm⁻² to 50 mA cm⁻². In addition, as seen in Fig. 2C, it was observed that the capacity utilization of these ferrocene catholytes was in the order of C_1 -FcNCl (e.g., 11.6 W h L⁻¹ at 40 mA cm⁻²) < C_3 -FcNCl (12.1 W h L⁻¹) < C_2 -FcNCl (12.6 W h L⁻¹). It is interpreted that the charge transfer resistance becomes impactful with the increased operational current as the charge transfer rate constants of these ferrocene catholytes are in the order of C_1 -FcNCl $< C_2$ -FcNCl (see Table 1). The coulombic efficiencies of all the three half-cell RFBs at each current density were nearly 100%.

Cycling stability is one of the most essential properties of a redox active electrolyte, as it directly determines the lifetime

Table 1 Solubility, charge capacity, molar ion conductivity, reduction potentials, and electrochemical kinetics data of C_x -FcNCl in aqueous solutions at room temperature

Compound	Solubility, M (capacity, Ah L ⁻¹)	Molar ion conductivity ($\Lambda_{\rm m}$, S cm ² mol ⁻¹)	$E_{1/2}$, V (vs. NHE)	k^0 , cm s ⁻¹	D , cm 2 s $^{-1}$
C ₁ -FcNCl	4.00 (107.2)	63.0	0.61	0.126	6.80×10^{-6}
C_2 -FcNCl	2.60 (69.7)	63.7	0.44	0.288	6.10×10^{-6}
C_3 -FcNCl	2.30 (61.6)	61.4	0.37	0.193	5.78×10^{-6}

Redox potentials and electrochemical kinetics were tested in 0.50 M NH₄Cl aqueous solution.

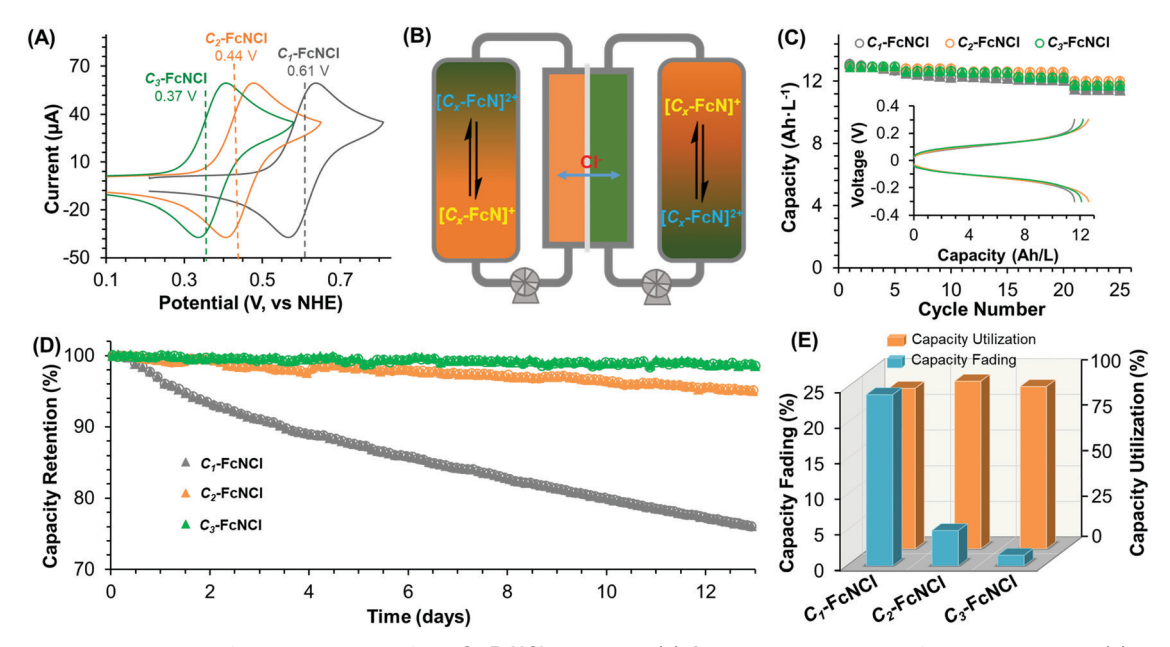


Fig. 2 Cyclic voltammetry and half-cell RFB studies of the Cx-FcNCl catholytes. (A) Cyclic voltammograms of the Fc derivatives; (B) the scheme of C_x-FcNCl half-cell RFBs; (C) charge (○) and discharge (▲) capacity versus cycling number at from 10 to 50 mA cm⁻² current densities for 0.50 M C₁-FcNCl (gray), C2-FcNCl (orange), and C3-FcNCl (green) half-cell RFBs; Inset: Representative charge and discharge profiles at 40 mA cm⁻²; (D) capacity retention of 0.50 M C_x -FcNCl half-cell RFBs at 40 mA cm⁻² during 13 testing days: C_1 -FcNCl (gray), C_2 -FcNCl (orange), and C_3 -FcNCl (green); (E) comparison of initial capacity utilization (orange) and capacity fading percentages (blue) of the C_x -FcNCl half-cell RFBs at 40 mA cm⁻² in 13 testing days. CV conditions: 2 mM C_x -FcNCl in 0.50 M NH₄Cl aqueous solution, 100 mV s⁻¹ scan rate, glassy carbon working and counter electrodes, Ag/AgCl reference electrode. RFB conditions: catholyte, 0.50 M Cx-FcNCl in 1.00 M NH4Cl; anolyte, 0.50 M [Cx-FcNCl] in 1.0 M NH4Cl; Selemion AMV anionexchange membrane; 25 °C

Table 2 Long-term cycling performance of the C_x -FcNCl half-cell RFBs and C_x -FcNCl/(NPr)₂VCl₄ full-cell AORFBs at 40 mA cm⁻²

	Cycle number	Capacity fading (%)	Fading ra	Fading rate	
Material			% per day	% per cycle	
C_1 -FcNCl C_2 -FcNCl C_3 -FcNCl C_1 -FcNCl/ (NPr) $_2$ VCl $_4$ C_2 -FcNCl/ (NPr) $_2$ VCl $_4$ C_3 -FcNCl/ (NPr) $_3$ VCl $_4$	585 527 508 500 500	23.99 4.95 1.85 13.53 2.57	1.85 0.38 0.14 1.03 0.18	0.041 0.009 0.004 0.027 0.005	

and energy storage cost of RFBs. To validate the cycling stability of the C_x -FcNCl catholytes, the half-cell RFBs were continually operated at 40 mA cm⁻² for 13 days (Fig. 2D and Fig. S4-S6, ESI† for detail). Initial capacity utilization of the half-cell RFBs was 90.3% for C_1 -FcNCl, 94.1% for C_2 -FcNCl, and 91.4% for C_3 -FcNCl, respectively (Fig. 2E). In 13 testing days, C_2 -FcNCl and C_3 -FcNCl half-cell RFBs delivered excellent cycling stability; specifically, only 4.95% and 1.85% capacity fading was observed, equivalent to 0.381% and 0.14% per day capacity fading rate, respectively. However, significant capacity decay was observed in the C_1 -FcNCl half-cell RFB (23.99% capacity fading, equivalent to 1.85% per day fading rate). CV and ¹H-NMR post-cycling analyses were conducted to understand the possible chemical degradation of the C_x -FcNCl electrolytes

in the cycling process. As shown in Fig. S8-S10 (ESI†), ¹H-NMR spectra and CV curves of cycled C_2 -FcNCl and C_3 -FcNCl remained unchanged. However, a new peak at δ = 2.81 ppm was observed in the 1 H-NMR spectrum of the cycled C_{1} -FcNCl electrolyte (Fig. S7, ESI†), which is assigned to the dissociated (2,4-cyclopentadiene-1-methyl)trimethylammonium Decomposition of the C_1 -FcNCl electrolyte was further confirmed by the remarkable peak intensity decrease in the postcycling CV analysis (Fig. S10A, ESI†). Noticeably, Fe(OH)₃ was identified as an orange solid on the surface of electrodes and separator of the C_1 -FcNCl half-cell RFB after long-term cycling and confirmed by EDS tests (Fig. S11, ESI†). However, no apparent Fe(OH)3 was observed in the cycled C2-FcNCl and C_3 -FcNCl half-cell RFBs (Fig. S12, ESI†), consistent with the half-cell RFB results.

We also performed full-cell AORFB studies of the C_x -FcNCl catholytes by pairing with 1,1'-di(trimethylammonium-propyl) 4,4'-bipyridium tetrachloride, $[(NPr)_2V]Cl_4$ ($E_{1/2} = -0.38 \text{ V versus}$ NHE, Table 2), which has been reported as a robust viologen anolyte in viologen/ferrocene and viologen/TEMPO AORFBs. 6,8,10 The same trend of cycling stability as the halfcell RFBs was observed; specifically, C1-FcNCl/(NPr)2VCl4 AORFB showed much poorer stability than C_2 -FcNCl/(NPr)₂VCl₄ and C3-FcNCl/(NPr)2VCl4 AORFBs (see ESI† for detail). In 500 charge/discharge cycles at 40 mA cm⁻², capacity fading of 13.53% was obtained in C_1 -FcNCl/(NPr)₂VCl₄ AORFB. However, only 2.57% and 1.03% capacity fading was observed in the C_2 -FcNCl/(NPr)₂VCl₄ and C_3 -FcNCl/(NPr)₂VCl₄ AORFBs,

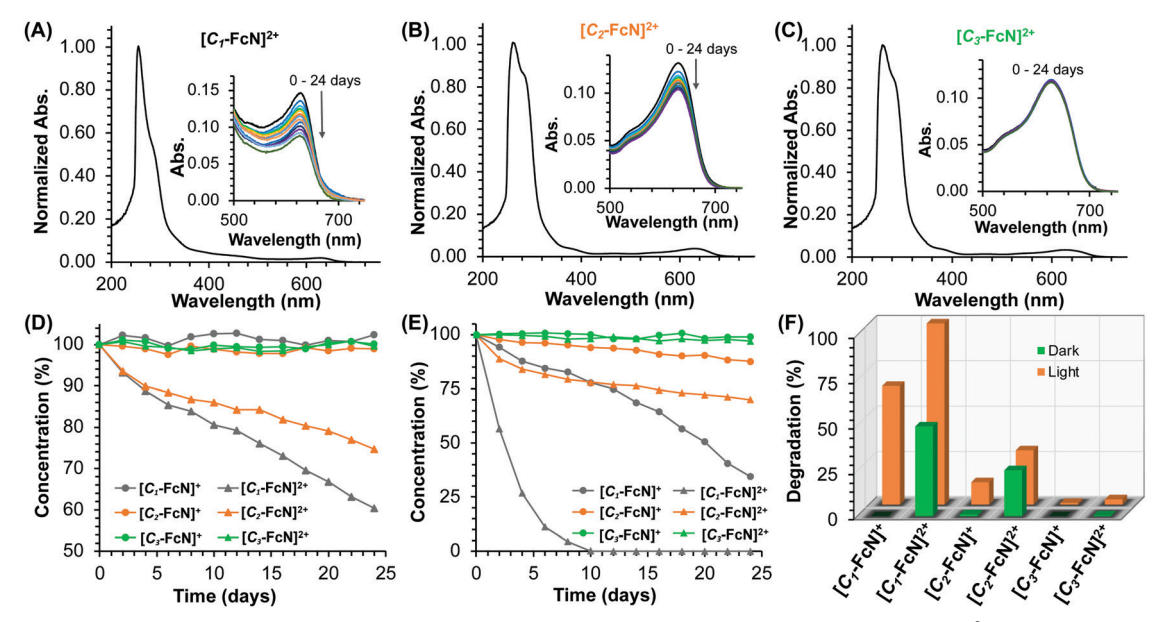


Fig. 3 UV-Vis stability studies of the C_x -FcNCl catholytes in N_2 atmosphere for 24 days. (A) Charged state $[C_1$ -FcN]²⁺ under dark; (B) charged state $[C_2-FcN]^{2+}$ under dark; (C) charged state $[C_3-FcN]^{2+}$ under dark; (D) concentration change of charged state and discharged state $C_3-FcN]^{2+}$ under dark; (E) concentration change of charged state and discharged state C_x -FcNCl catholytes under light; (F) comparison of the degradation percentages

respectively (Fig. S13-S15, ESI†). The capacity fading rate is equivalent to 1.03% per day for C₁-FcNCl/(NPr)₂VCl₄ AORFB. However, only 0.18% per day for the C2-FcNCl/(NPr)2VCl4 AORFB and 0.073% per day for the C_3 -FcNCl/(NPr)₂VCl₄ AORFB.

Based on the battery testing results, the stability of C_x -FcNCl catholytes and their charged states in aqueous solutions was further investigated with UV-Vis measurements (Fig. 3A-C and Fig. S23-S25, ESI†). Three absorptions were observed for the charged state, $[C_x\text{-FcN}]^{2+}$, 259 nm (MLCT), 295 nm (LMCT), 653 (d-d) for $[C_1$ -FcN]²⁺ (Fig. 3A), 274 nm (MLCT), 291 nm (LMCT), 357 (d-d), 647 (d-d) for $[C_2\text{-FcN}]^{2+}$ (Fig. 3B), and 259 nm (MLCT), 295 nm (LMCT), 639 (d-d) for $[C_3\text{-FcN}]^{2+}$ (Fig. 3C). As shown in Fig. 3D, F and Fig. S23A, S24A and S25A (ESI†), the discharged states, $[C_x$ -FcN]⁺, are highly stable, as minor decomposition was detected after standing for 24 days under dark in an N₂ atmosphere. However, by monitoring the d-d transition absorption, the charged state $[C_1$ -FcN $]^{2+}$ and

 $[C_2$ -FcN]²⁺ showed 49.6% or 2.06% per day and 25.4% or 1.05% per day decomposition in 24 days, respectively. In stark contrast, the charged state, $[C_3$ -FcN]²⁺, is significantly more stable (only 0.5% or 0.02% per day) (Fig. 3A-D). It is noted that the degradation rates measured in the UV-Vis studies are consistent with the capacity fading rates obtained by the halfcell studies. The influence of light on the stability of C_x -FcNCl catholytes was also studied by UV-Vis tests. As shown in Fig. 3E and F, the degradation of the charged state $[C_r\text{-FcN}]^{2+}$ species was even accelerated by ambient light exposure. Specifically, $[C_1$ -FcN]²⁺ was fully decomposed in 10 days, 30.1% and 3.0% decomposition were detected for $[C_2\text{-FcN}]^{2+}$ and $[C_3\text{-FcN}]^{2+}$ species, respectively. To our surprise, the discharged state $[C_1$ -FcN]⁺ and $[C_2$ -FcN]⁺ species are also light-sensitive, as 65.5% and 12.4% decomposition were observed, respectively, after 24 days of light exposure while no apparent decomposition observed for C_3 -FcNCl. Overall, was

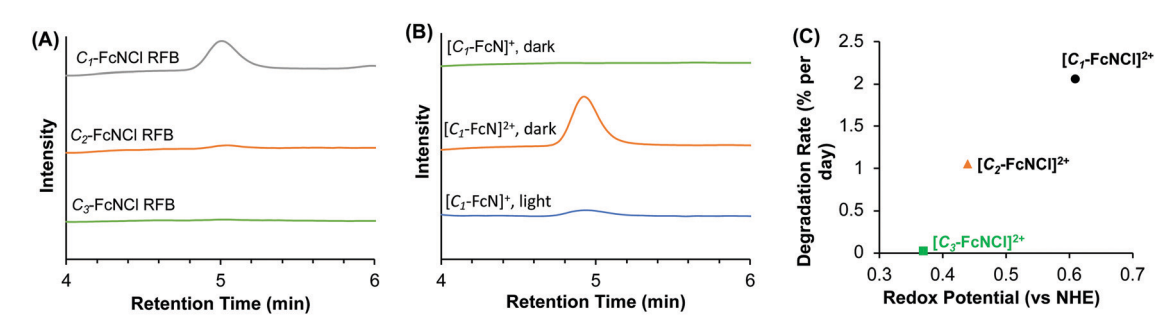


Fig. 4 Gas chromatography (GC) studies and correlation of redox potential and stability. (A) GC curves of the gas phase samples collected from electrolyte reservoirs of the C_x -FcNCI half-cell RFBs after 13 days of cycling. (B) GC curves of gas phase samples upon keeping 0.50 M discharged state [C₁-FcN]⁺ and charged state [C₁-FcN]²⁺ water solutions in sealed vials for 5 days. (C) The correlation of the degradation rate of the charged state $[C_x$ -FcN]²⁺ series measured by UV-Vis vs. their redox potential.

C₃-FcNCl catholyte delivered the best thermal- and photostability under both charged and discharged states among these Fc derivatives.

To gain a further understanding of the degradation mechanism of the C_x -FcNCl catholytes in AORFBs, gas phase samples were collected from the electrolyte reservoirs of the half-cell RFBs after long-term cycling tests for gas chromatography (GC) studies. As shown in Fig. 4A, signals with a retention time of 4.98 min were observed in the GC curves of C_1 -FcNCl and C_2 -FcNCl samples. It was further characterized by GC-MS (Fig. S26, ESI†), and a signal of m/z = 66.0 was detected, indicating the formation of free cyclopentadiene (C₅H₆). Then, we further conducted GC tests with the gas phase samples collected from vials sealed with discharged state $[C_1$ -FcN]⁺ and charged state $[C_1$ -FcN $]^{2+}$. As shown in Fig. 4B, no free C_5H_6 was detected from the $[C_1$ -FcN]⁺ sample after standing in the dark for 5 days (green curve). However, C₅H₆ was detected from the samples of $[C_1\text{-FcN}]^{2+}$ under dark (orange curve) and $[C_1\text{-FcN}]^+$ under light (blue curve). These findings are consistent with the results of UV-Vis studies.

Besides the thermal- and photo-induced degradation of C_x -FcNCl catholytes, we observed that the cycling stability of C_1 -FcNCl half-cell RFB was sensitive to O_2 . As shown in Fig. S27 (ESI†), when the environmental O2 content was increased to 20 ppm, dramatic decay of the battery capacity was observed. UV-Vis studies indicate that O2 could accelerate the degradation of the charged state $[C_1$ -FcN $]^{2+}$ (Fig. S28, ESI \dagger). It was also found that the electron-rich discharged states, $[C_2\text{-FcN}]^+$ and $[C_3\text{-FcN}]^+$, can be partially oxidized by O_2 . However, the discharged state $[C_1$ -FcN]⁺ and charged state $[C_2$ -FcN]²⁺ and $[C_3$ -FcN]²⁺ were not sensitive to O_2 (Fig. S28-S30, ESI†).

Discussion

According to the above experimental results, it is reasonable to conclude that thermal-induced Cp ligand dissociation of the charged state Fc⁺ is a credible degradation pathway under the

dark conditions for the Fc catholytes in AORFBs. It is also reasonable to argue that the 18-electron configuration of the discharged state, Fc, is much more stable than the 17-electron configuration of Fc^+ . Within the C_x -FcNCl series, thermal ligand dissociation takes place in the order of $[C_1$ -FcN $]^{2+}$ > $[C_2\text{-FcN}]^{2+} > [C_3\text{-FcN}]^{2+}$, consistent with the ligand strength order of C_1 -Cp⁻ $< C_2$ -Cp⁻ $< C_3$ -Cp⁻. The degradation mechanism in the case of $[C_1\text{-FeN}]^{2+}$ is proposed in Scheme 1. After the dissociation of the C_1 -Cp ligand, the open site of the electrophilic Fe³⁺ center of Fc⁺ can be attacked by H₂O in an aqueous solution. The coordinated H₂O becomes more acidic. It is believed that intramolecular deprotonation by the dissociated C_1 -Cp⁻ anion ligand leads to the formation of the protonated product, (trimethylammonium)methyl cyclopentadiene. The other plain Cp ligand will undergo the same reaction and eventually lead to the formation of the Fe(OH)3 precipitate. Particularly, C_1 -FcNCl with the least donating C_1 -Cp ligand experienced the fastest degradation. Regarding battery performance, the cycling stability is primarily limited by the charged state.

Under the light condition, it is believed the metal-to-ligand charge transfer (MLCT) activates the bonding between the Fe²⁺ or Fe3+ center and the Cp ligands and triggers the photoinduced ligand dissociation. Photolytic ligand dissociation is greater than the thermal ligand dissociation as even the discharged state (the oxidation state of Fe²⁺) such as $[C_3$ -FcN]⁺ becomes unstable. Then subsequent reactions are similar to those in the thermal degradation. Thereby, avoiding light exposure is critical to mitigating the photolytic ligand dissociation and should be aware of in future flow battery studies.

For the future development of coordination compound electrolytes, it is important to develop a strong ligand-metal coordination sphere that could alleviate the performance decay of coordination catholyte molecules. It is also noticed that the redox potential can serve as a reporter for the ligand strength and is consistent with the degradation rate of the C_x -FcNCl series (Fig. 4C) measured by UV-Vis tests. The redox potential and chemical stability of the C_x -FcNCl series can serve as the benchmark for future coordination compound electrolytes. It is

$$[C_{T}FcN]^{2+}$$

$$\begin{array}{c} & & & & \\ & &$$

Scheme 1 Proposed thermal degradation mechanism of $[C_1$ -FcN $]^{2+}$, the charged state of C_1 -FcNCI.

worth noting that within the C_x -FcNCl series, the increased ligand-metal coordination stability scarifies the oxidation potential, *e.g.*, C_3 -FcNCl (0.37 V, stable) *versus* C_1 -FcNCl (0.61 V, unstable). In addition, electron rich C_3 -FcNCl becomes more O_2 sensitive than C_1 -FcNCl. Thus, it is important to exclude O_2 induced side reactions in flow battery studies.

Conclusions

In summary, we reported the detailed degradation mechanism of a series of ferrocene catholytes in pH-neutral AORFBs. Thermal- and photo-induced C_x -Cp⁻ ligand dissociation pathways of the charged state (Fc+) and light-excited state (Fc+) species were experimentally confirmed. Electron-withdrawing functional groups weaken the coordination between the Fe³⁺ or Fe^{2+} center and the C_x - Cp^- ligand of the charged state and light-excited state. Thus, the C_x -Cp⁻ ligands can be irreversibly replaced by nucleophiles. However, electron-donating groups stabilize the Fe³⁺ or Fe²⁺ center of the Fc molecules and hinder the thermal- and photo-induced ligand dissociation reactions. This work not only reveals the structure-performance relationship and degradation mechanisms of the Fc catholytes in aqueous electrolytes but also provides important guidance for the design of high-performance Fc and other coordination compound electrolytes and the operation condition of flow batteries.

Experimental section

Chemicals and manipulations

All chemicals were purchased from Sigma-Aldrich, TCI, and Oakwood, stored in an argon filled glove box and used directly. Deionized water was degassed by purging with N₂ before use. All experimental operations were conducted under an N2 atmosphere. Conductivities and pH values of the electrolytes were measured using a Mettler Toledo conductivity meter or a Mettler Toledo pH meter at room temperature. ¹H-NMR spectra were collected using a Bruker 500 MHz NMR spectrometer. Elemental analysis was performed by Atlantic Microlab. FT-IR spectra were collected on a PerkinElmer Spectrum 100 FT-IR spectrometer with a universal ATR sampling accessory. UV-Vis spectra were collected using an Agilent Cary 100 UV-Vis spectrometer. Gas chromatography (GC) was measured via an SRI gas chromatography system 8610C equipped with a molecular sieve 13× packed column, a HayesSep D packed column, and a flame ionization detector (FID) using argon as the carrier gas. The GC-MS measurements were conducted in a Shimadzu GCMS-QP5000 system using helium as the carrier gas. Energy dispersive spectroscopy (EDS) measurement was conducted on an FEI Quanta 650 (FEI, USA) at the Microscopy Core Facility of Utah State University (WD 10 mm, voltage 10-20 kV). All electrochemical experiments were conducted with Gamry 5000E or 1000E potentiostat. Battery tests were conducted using a Land battery testing system.

Synthesis of (ferrocenylmethyl)trimethylammonium chloride (C₁-FcNCl)

Iodomethane (CH₃I, 3.7 mL, 60.0 mmol, 1.2 equiv.) in 100.0 mL diethyl ether was added dropwise to a solution of N, N-dimethylaminomethylferrocene (12.2 g, 50.0 mmol, 1.0 equiv.) in 300.0 mL diethyl ether under rapid stirring at 0 °C. After stirring the reaction mixture at room temperature for 6 h, the produced orange precipitate was filtered, washed with 3 \times 50.0 mL diethyl ether, and dried under vacuum. The iodide salt was converted to chloride salt by anion exchange. The C_1 -FcNCl product was obtained as a bright yellow powder, 14.4 g (98% yield). The 1 H-NMR spectrum and elemental analysis data are the same as previously reported.

Synthesis of (ferrocenylethyl)dimethylamine

^tBuLi (66.0 mL, 1.7 M in hexane, 1.05 equiv.) solution was added dropwise into a solution of ferrocene (20.0 g, 107.0 mmol, 1.0 equiv.) in 200.0 mL dry THF at 0 °C. The reaction mixture was warmed up to room temperature and stirred for 30 min. And then, a solution of 2-chloro-N,N-dimethylethylamine (13.9 g, 128.0 mmol, 1.2 equiv.) in 40.0 mL dry THF was added dropwise at 0 °C. After stirring for another 14 h at room temperature, 5.0 mL H₂O was carefully added to quench the reaction. The mixture was dried under a vacuum. The residue was dissolved in a 250.0 mL 1.0 M HCl solution and washed with 150.0 mL hexane three times. Then, the pH of the aqueous solution was turned to > 7.0 and extracted with 3 \times 200.0 mL CH₂Cl₂. The organic phase was combined and dried with Na₂SO₄. The solvent was removed to give the product as a deep brown liquid (18.2 g, 66% yield). 1 H-NMR (CDCl₃, 500 MHz): δ (ppm), 2.35 (s, 6H), 2.49-2.61 (m, 4H), 4.01-4.21 (m, 9H).

Synthesis of (2-ferrocenyl-ethyl)trimethylammonium chloride $(C_2$ -FcNCl)

Iodomethane (CH₃I, 3.7 mL, 60.0 mmol, 1.2 equiv.) in 100.0 mL diethyl ether was added dropwise to a solution of (ferrocenylethyl)dimethylamine (12.9 g, 50.0 mmol, 1.0 equiv.) in 300.0 mL diethyl ether under rapid stirring at 0 °C. The reaction mixture was stirred at room temperature for 6 h. The resulting orange precipitate was filtered, washed with 50.0 mL diethyl ether three times, and dried under vacuum. The C_2 -FcNCl product was obtained through anion-exchange as an orange powder (15.0 g, 98% yield). 1 H-NMR (D₂O, 500 MHz): δ (ppm), 2.41 (m, 4H), 2.83 (t, J = 8.0 Hz, 2H), 3.09 (s, 9H), 3.42 (d, J = 8.5 Hz, 2H), 4.08–4.27 (m, 9H). Elemental analysis for C_2 -FcNCl, Calculated: C 58.56, H 7.21, N 4.55. Found: C 58.48, H 7.47, N 4.46.

Synthesis of 3-chloro-propylferrocene

A solution of 3-chloropropanoyl chloride (13.0 g, 102.0 mmol, 1.02 equiv.) in 50.0 mL dry $\rm CH_2Cl_2$ was added into a suspension of $\rm AlCl_3$ (14.7 g, 110.0 mmol, 1.1 equiv.) in 100.0 mL dry $\rm CH_2Cl_2$. After stirring at room temperature for 2 h, the mixture was transferred into a solution of ferrocene (18.6 g, 100.0 mmol, 1.0 equiv.) in 150.0 mL dry $\rm CH_2Cl_2$ at 0 °C. The reaction mixture

was warmed up to room temperature and stirred overnight. Then, the mixture was cooled to 0 °C again, and a solution of NaBH₄ (3.8 g, 100.0 mmol, 1.0 equiv.) in 50.0 mL diglyme was added. After stirring at room temperature for another 4 h, the mixture was quenched with 150.0 mL 1.00 M HCl solution and extracted with 100.0 mL CH₂Cl₂ three times. The organic phase was combined and dried with Na2SO4. After removal of the solvent, the product was obtained as a deep brown liquid. 21.8 g, 83% yield. ${}^{1}\text{H-NMR}$ (CDCl₃, 500 MHz): δ (ppm), 1.78-2.17 (m, 2H), 2.25-2.66 (m, 2H), 3.36-3.76 (m, 2H), 3.91-4.41 (m, 9H).

Synthesis of (3-ferrocenyl-propyl)trimethylammonium chloride $(C_3$ -FcNCl)

3-Chloro-propylferrocene (2.6 g, 10.0 mmol, 1.0 equiv.) and Me₃N in THF solution (2.00 M, 25.0 mL, 5.0 equiv.) were sealed in an autoclave (8 autoclaves were simultaneously setup). The reactors were kept at 85 °C for 3 days. The C_3 -FcNCl product was obtained through filtration as orange powder. 22.7 g, 88% yield. 1 H-NMR (D₂O, 500 MHz): δ (ppm), 1.86–1.98 (m, 2H), 2.33-2.47 (m, 2H), 3.02 (m, 9H), 3.25 (t, I = 7.5 Hz, 2H), 3.67–4.66 (m, 9H). Elemental analysis for C_3 -FcNCl, calculated: C 59.74, H 7.52, N 4.35. Found: C 59.63, H 7.71, N 4.28.

Cyclic voltammetry

All CV measurements were conducted in 0.50 M NH₄Cl electrolyte solutions under N2 atmosphere using a Gamry 1000E potentiostat with a three-electrode system: a PEEK-encased 3.0 mm diameter glassy carbon working electrode, a glassy carbon rod counter electrode, and an Ag/AgCl reference electrode. Before each CV scan, the working electrode was cleaned by polishing with 0.05 micron alumina powder and rinsing with deionized water. Potential values were corrected to NHE using a methyl viologen (MV2+) internal standard with a known redox potential at -0.45 V vs. NHE.

Levich equation to measure the diffusion coefficient (D)

The linear sweep voltammetry (LSV) studies were conducted using a Gamry 5000E potentiostat in a three-electrode configuration, a 5.0 mm Teflon-encased glassy carbon disc working electrode (Pine Research Instrumentation), a glassy carbon rod counter electrode, and an Ag/AgCl reference electrode. Before each measurement, the working electrode was polished with 0.05 micron alumina powder and rinsed with deionized water. The electrode was rotated from 300 to 2400 rpm with an increment of 300 rpm using a Pine MSR rotation controller. LSV curves were collected at 5 mV s⁻¹ scan rate. At each rotation rate, the LSV was recorded three times to ensure repeatability.

Diffusion coefficients (D) were obtained from the slopes of Levich plots based on the RDE data of 1.0 mM C_x -FcNCl in 0.50 M NH₄Cl. The Levich equation is written as:

$$i = (0.620)nFAC_0D^{2/3}\omega^{1/2}v^{-1/6}$$
 (1)

where i is the limiting current density from the RDE tests, A is the area of the RDE (glassy carbon, 0.196 cm^2), n is the number of charges (n = 1), F is 96 485 C mol⁻¹, C_0 is the concentration of compounds ($C_0 = 1.0 \times 10^{-6} \text{ mol cm}^{-3}$), D is the diffusion coefficient (cm² s⁻¹), ω is the angular rotation rate of the electrode, and v is the kinematic viscosity (0.0100 cm² s⁻¹ for 0.50 M NH₄Cl solution).

The slope of $i - \omega^{1/2}$ curve is $(0.620)nFAC_0D^{2/3}v^{-1/6}$.

Nicholson's method to estimate electron transfer rates constants (k^0)

Following the Nicholson's method, CV curves of 4.0 mM C_r -FcNCl in 0.50 M NH₄Cl were collected at a scan rate range of 5 500 mV s⁻¹. The kinetic parameter, Ψ , was calculated by the potential gap between reductive and oxidative peaks (peakto-peak separation, ΔE_p) through eqn (2). And then, based on the relationship between Ψ and $v^{-1/2}$ (eqn (3)), k^0 was calculated using the slope of Ψ vs. $v^{-1/2}$ plot.

$$\Psi = (-0.6288 + 0.0021\Delta E_{\rm p})/(1 - 0.017\Delta E_{\rm p})$$
 (2)

$$\Psi = k^0 \left[\pi D n F / R T \right]^{-1/2} v^{1/2} \tag{3}$$

where F, D, and n are defined in eqn (1), and v represents the scan rate.

Half-cell flow battery tests

The half-cell RFBs were constructed with two carbon electrolyte chambers, two graphite felt electrodes (SGL Carbon Group, Germany), a piece of Selemion AMV anion-exchange membrane sandwiched between the graphite felts. Two copper plates were used as current collectors. Each carbon chamber was connected with an electrolyte reservoir using a piece of Viton tubing. The electrolyte reservoir is home designed and is a 10.0 mL glass tube (2 cm inner diameter). The active area of the cell was 10 cm². A Masterflex L/S peristaltic pump (Cole-Parmer, Vernon Hills, IL) was used to press the Viton tubing to circulate the electrolytes through the electrodes at a flow rate of 60.0 mL·min⁻¹. In each side of the battery, 12.0-13.0 mL of 1.00 M NH₄Cl electrolyte containing 0.50 M active material was employed. The flow cell was galvanostatically charged/discharged at room temperature within the voltage range of -0.30-0.30 V under 10 to 50 mA cm⁻² current density. Postcell studies of the C_x -FcNCl electrolytes were conducted after full discharge.

Full-cell flow battery tests

The setup of C_x -FcNCl/(NPr)₂VCl₄ AORFBs is the same as the half-cell batteries. In each battery, 12.0-13.0 mL 0.5 M C_x-FcNCl and 0.5 M (NPr)₂VCl₄ with 1.0 M NH₄Cl supporting electrolyte were used as a catholyte and an anolyte, respectively. The batteries were galvanostatically charged/discharged within the voltage range of 0.10-1.30 V for the C_1 -FcNCl/(NPr)₂VCl₄ RFB, 0.10-1.20 V for the C2-FcNCl/(NPr)2VCl4 RFB, and 0.10-1.05 V for the C3-FcNCl/(NPr)2VCl4 AORFB at current densities of $10 \text{ mA cm}^{-2} \text{ to } 50 \text{ mA cm}^{-2}$.

Conflicts of interest

Reported ferrocence electrolytes used for redox flow batteries were included in a filed patent (United States patent No., 10 934 258).

Acknowledgements

We thank National Science Foundation (Career Award, Grant No. 1847674) and Utah State University (faculty startup funds to Dr T. Leo Liu) for supporting this study. M. H. is grateful for China CSC Abroad Studying Fellowship to support her study at Utah State University. We acknowledge that the NMR studies are supported by NSF's MRI program (award number 1429195).

References

- 1 J. Luo, B. Hu, M. Hu, Y. Zhao and T. L. Liu, Status and Prospects of Organic Redox Flow Batteries towards Sustainable Energy Storage, ACS Energy Lett., 2019, 4, 2220–2236.
- 2 B. Hu, J. Luo, C. Debruler, M. Hu, W. Wu and T. L. Liu, Redox-Active Inorganic Materials for Redox Flow Batteries, *Encyclopedia of Inorganic and Bioinorganic Chemistry*, 2019, pp. 1–25, DOI: 10.1002/9781119951438.eibc2679.
- 3 Y. Ding, C. Zhang, L. Zhang, Y. Zhou and G. Yu, Molecular Engineering of Organic Electroactive Materials for Redox Flow Batteries, *Chem. Soc. Rev.*, 2017, 47, 69–103.
- 4 X. Wei, W. Pan, W. Duan, A. Hollas, Z. Yang, B. Li, Z. Nie, J. Liu, D. Reed, W. Wang and V. Sprenkle, Materials and Systems for Organic Redox Flow Batteries: Status and Challenges, *ACS Energy Lett.*, 2017, 2, 2187–2204.
- 5 J. Winsberg, T. Hagemann, T. Janoschka, M. D. Hager and U. S. Schubert, Redox-Flow Batteries: From Metals to Organic Redox-Active Materials, *Angew. Chem., Int. Ed.*, 2016, 56, 686–711.
- 6 T. Liu, B. Hu, C. Debruler and J. Luo, *Materials for Use in an Aqueous Organic Redox Flow Battery*, U.S. Patent, 10934258, 2021.
- 7 B. Hu, C. DeBruler, Z. Rhodes and T. L. Liu, Long-Cycling Aqueous Organic Redox Flow Battery (AORFB) toward Sustainable and Safe Energy Storage, *J. Am. Chem. Soc.*, 2017, 139, 1207–1214.
- 8 C. DeBruler, B. Hu, J. Moss, X. Liu, J. Luo, Y. Sun and T. L. Liu, Designer Two-Electron Storage Viologen Analyte Materials for Neutral Aqueous Organic Redox Flow Batteries, *Chemistry*, 2017, 3, 1–18.
- 9 J. Luo, B. Hu, C. Debruler, Y. Bi, Y. Zhao, B. Yuan, M. Hu, W. Wu and T. L. Liu, Unprecedented Capacity and Stability of Ammonium Ferrocyanide Catholyte in pH Neutral Aqueous Redox Flow Batteries, *Joule*, 2019, 3, 1–15.
- 10 E. S. Beh, D. De Porcellinis, R. L. Gracia, K. T. Xia, R. G. Gordon and M. J. Aziz, A Neutral pH Aqueous Organic-Organometallic Redox Flow Battery with Extremely High Capacity Retention, ACS Energy Lett., 2017, 2, 639-644.
- 11 Y. Xu, Y.-H. Wen, J. Cheng, G.-P. Cao and Y.-S. Yang, A Study of Tiron in Aqueous Solutions for Redox

- Flow Battery Application, *Electrochim. Acta*, 2010, 55, 715–720.
- 12 B. Huskinson, M. P. Marshak, C. Suh, S. Er, M. R. Gerhardt, C. J. Galvin, X. Chen, A. Aspuru-Guzik, R. G. Gordon and M. J. Aziz, A Metal-Free Organic-Inorganic Aqueous Flow Battery, *Nature*, 2014, 505, 195–198.
- 13 B. Yang, L. Hoober-Burkhardt, F. Wang, G. K. Surya Prakash and S. R. Narayanan, An Inexpensive Aqueous Flow Battery for Large-Scale Electrical Energy Storage Based on Water-Soluble Organic Redox Couples, *J. Electrochem. Soc.*, 2014, 161, A1371–A1380.
- 14 B. Hu, J. Luo, M. Hu, B. Yuan and T. L. Liu, A pH Neutral, Metal Free Aqueous Organic Redox Flow Battery Employing an Ammonium Anthraquinone Anolyte, *Angew. Chem., Int. Ed.*, 2019, **58**, 16629–16636.
- 15 Z. Yang, L. Tong, D. P. Tabor, E. S. Beh, M.-A. Goulet, D. De Porcellinis, A. Aspuru-Guzik, R. G. Gordon and M. J. Aziz, Alkaline Benzoquinone Aqueous Flow Battery for Large-Scale Storage of Electrical Energy, *Adv. Energy Mater.*, 2018, 8, 1702056.
- 16 J. B. Gerken, C. W. Anson, Y. Preger, P. G. Symons, J. D. Genders, Y. Qiu, W. Li, T. W. Root and S. S. Stahl, Comparison of Quinone-Based Catholytes for Aqueous Redox Flow Batteries and Demonstration of Long-Term Stability with Tetrasubstituted Quinones, Adv. Energy Mater., 2020, 10, 2000340.
- 17 K. Lin, R. Gómez-Bombarelli, E. S. Beh, L. Tong, Q. Chen, A. Valle, A. Aspuru-Guzik, M. J. Aziz and R. G. Gordon, A Redox-Flow Battery with An Alloxazine-based Organic Electrolyte, *Nat. Energy*, 2016, 1, 16102.
- 18 A. Hollas, X. Wei, V. Murugesan, Z. Nie, B. Li, D. Reed, J. Liu, V. Sprenkle and W. Wang, A Biomimetic High-capacity Phenazine-based Anolyte for Aqueous Organic Redox Flow Batteries, *Nat. Energy*, 2018, 3, 508–514.
- 19 C. Zhang, Z. Niu, S. Peng, Y. Ding, L. Zhang, X. Guo, Y. Zhao and G. Yu, Phenothiazine-Based Organic Catholyte for High-Capacity and Long-Life Aqueous Redox Flow Batteries, *Adv. Mater.*, 2019, 31, 1901052.
- 20 S. Pang, X. Wang, P. Wang and Y. Ji, Biomimetic Amino Acid Functionalized Phenazine Flow Batteries with Long Lifetime at Near-Neutral pH, *Angew. Chem., Int. Ed.*, 2021, 60, 5289–5298.
- 21 T. Janoschka, N. Martin, M. D. Hager and U. S. Schubert, An Aqueous Redox-Flow Battery with High Capacity and Power: The TEMPTMA/MV System, *Angew. Chem., Int. Ed.*, 2016, 55, 14427–14430.
- 22 Y. Liu, M.-A. Goulet, L. Tong, Y. Liu, Y. Ji, L. Wu, R. G. Gordon, M. J. Aziz, Z. Yang and T. Xu, A Long-Lifetime All-Organic Aqueous Flow Battery Utilizing TMAP-TEMPO Radical, *Chem*, 2019, 5, 1861–1870.
- 23 T. Liu, X. Wei, Z. Nie, V. Sprenkle and W. Wang, A Total Organic Aqueous Redox Flow Battery Employing a Low Cost and Sustainable Methyl Viologen Anolyte and 4-HO-TEMPO Catholyte, Adv. Energy Mater., 2016, 6, 1501449.
- 24 M. J. Baran, M. N. Braten, S. Sahu, A. Baskin, S. M. Meckler, L. Li, L. Maserati, M. E. Carrington, Y.-M. Chiang,

- D. Prendergast and B. A. Helms, Design Rules for Membranes from Polymers of Intrinsic Microporosity for Crossover-free Aqueous Electrochemical Devices, *Joule*, 2019, 3, 2968–2985.
- 25 V. Medabalmi, M. Sundararajan, V. Singh, M.-H. Baik and H. R. Byon, Naphthalene Diimide as A Two-electron Anolyte for Aqueous and Neutral pH Redox Flow Batteries, *J. Mater. Chem. A*, 2020, 8, 11218–11223.
- 26 Y. Chen, M. Zhou, Y. Xia, X. Wang, Y. Liu, Y. Yao, H. Zhang, Y. Li, S. Lu, W. Qin, X. Wu and Q. Wang, A Stable and High-Capacity Redox Targeting-Based Electrolyte for Aqueous Flow Batteries, *Joule*, 2019, 3, 2255–2267.
- 27 Q. Chen, Y. Li, Y. Liu, P. Sun, Z. Yang and T. Xu, Designer Ferrocene Catholyte for Aqueous Organic Flow Batteries, *ChemSusChem*, 2021, **14**, 1295–1301.
- 28 B. Hu and T. L. Liu, Tanking up Energy Through Atypical Charging, *Science*, 2021, 372, 788–789.

- 29 R. Prins, A. R. Korswagen and A. G. T. G. Kortbeek, Decomposition of the Ferricenium Cation by Nucleophilic Reagents, *J. Organomet. Chem.*, 1972, 39, 335–344.
- 30 J. Luo, A. Sam, B. Hu, C. DeBruler, X. Wei, W. Wang and T. L. Liu, Unraveling pH Dependent Cycling Stability of Ferricyanide/Ferrocyanide in Redox Flow Batteries, Nano Energy, 2017, 42, 215–221.
- 31 Y. Yamaguchi, W. Ding, C. T. Sanderson, M. L. Borden, M. J. Morgan and C. Kutal, Electronic Structure, Spectroscopy, and Photochemistry of Group 8 Metallocenes, *Coord. Chem. Rev.*, 2007, **251**, 515–524.
- 32 N. Mohammadi, A. Ganesan, C. T. Chantler and F. Wang, Differentiation of Ferrocene D_{5d} and D_{5h} Conformers Using IR Spectroscopy, *J. Organomet. Chem.*, 2012, 713, 51–59.
- 33 R. S. Nicholson, Theory and Application of Cyclic Voltammetry for Measurement of Electrode Reaction Kinetics, *Anal. Chem.*, 1965, 37, 1351–1355.